Title
NUMERICAL SOLUTION OF THE CAPILLARY FREE SURFACE EQUATION ON A SQUARE

Author
Chen, Nai-Fu

Publication Date
1977-11-01

To be Submitted for Publication

LBL-6145
Preprint

NUMERICAL SOLUTION OF THE CAPILLARY FREE SURFACE EQUATION ON A SQUARE

Nai-Fu Chen and Paul Concus

November 1977

Prepared for the U. S. Department of Energy
under Contract W-7405-ENG-48
and by the National Aeronautics and Space
Administration under Contract Number 67705-C

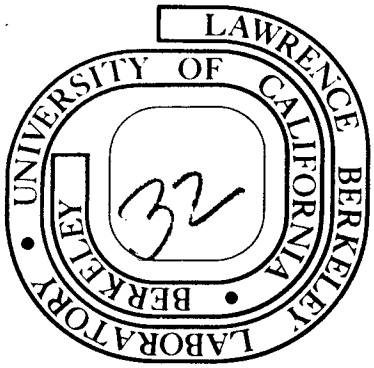

LBL-6145

DISCLAIMER

NUMERICAL SOLUTION OF THE CAPILLARY FREE SURFACE EQUATION ON A SQUARE

Nai-Fu Chen* and Paul Concus

Lawrence Berkeley Laboratory
University of California
Berkeley, California 94720

November 1977

ABSTRACT

Numerical methods are discussed for solving the partial differential equation describing the equilibrium free surface of a liquid in a vertical cylindrical container whose cross section has corners. Both the cases for which the free surface is bounded and for which it climbs infinitely high at a corner are considered. For the model problem of a container with square cross section comparative results of numerical experiments are given for a nonlinear relaxation method, for a conjugate gradient method, and for several techniques for handling the corner singularity utilizing the known asymptotic form of the solution. Representative solution surfaces are depicted graphically.

---

*Present address: Mathematics Department, University of Southern California, Los Angeles, CA 90007.

1. Introduction

In this paper, we discuss algorithms for solving numerically the nonlinear partial differential equation describing the equilibrium free surface of a liquid under surface and gravitational forces. We are interested particularly in the case of a liquid partly filling a vertical cylinder, the cross section of which has corners. We assume that the surface height $u(x,y)$ is a single-valued smooth function of x and y, that there is sufficient liquid to cover the cylinder base entirely, and that the gravitational field is uniform and directed vertically downward. Then the function $u(x,y)$ satisfies

$$\frac{\partial}{\partial x}\left(\frac{1}{W}\frac{\partial u}{\partial x}\right) + \frac{\partial}{\partial y}\left(\frac{1}{W}\frac{\partial u}{\partial y}\right) = Bu + 2H, \qquad W = \left[1 + (\partial u/\partial x)^2 + (\partial u/\partial y)^2\right]^{\frac{1}{2}} \tag{1}$$

where $B = \rho_o g/\sigma$ with ρ_o the difference in densities between the gas and liquid phases, g the gravitational acceleration (positive when directed downward), and σ the gas-liquid interfacial surface tension. The quantity 2H is a constant determined, in general, by the shape of the cylinder cross section, the volume of liquid, and the boundary condition between the liquid surface and the cylinder wall. The mean curvature of the surface is H at points were u=0. We consider only the case $B > 0$. The parameter B is the (dimensionless) Bond number, if (1) is considered to habe been made nondimensional with respect to a characteristic length of unity.

Let the prescribed angle of contact between the liquid free-surface and the cylinder wall, measured interior to the liquid, be denoted by

the constant γ. This condition can be written as

$$\frac{1}{W}\frac{\partial u}{\partial n} = \cos\gamma \quad \text{at the cylinder wall,} \tag{2}$$

where $\partial u/\partial n$ is the derivative of u with respect to the outward normal. We consider here only the case of wetting liquids, $0 \leqslant \gamma < \pi/2$. (The complementary case of non-wetting liquids can be derived from it directly by means of a simple transformation.)

The value of the contact angle plays a crucial role in determining the qualitative nature of the solution when the domain under investigation contains corners. Let the interior angle of a corner be 2α; it is proved in [6,7] that the solution at the vertex of the corner is bounded if and only if $\alpha + \gamma \geqslant \pi/2$. For the case $\alpha + \gamma < \pi/2$ set $\kappa = \sin\alpha \sec\gamma$ and introduce polar coordinates ρ, θ with origin at the vertex and θ measured from the interior angle bisector. Consider the function

$$v(x,y;\gamma) = \left[\cos\theta - (\kappa^2 - \sin^2\theta)^{\frac{1}{2}}\right]/(\kappa B\rho), \tag{3}$$

for $-\alpha \leqslant \theta \leqslant \alpha$, $\rho > 0$. It is shown in [5] that there exists a constant C such that the solution $u(x,y)$ satisfies $\left|u(x,y) - v(x,y)\right| < C$ for sufficently small ρ. Because of the differing qualitative natures of the bounded and unbounded solutions, we treat these two cases separately.

We take the 2 x 2 square as the domain for our model problem. Because of the symmetry, we consider only the equivalent problem on a 1 x 1 square with boundary conditions as shown in Figure 1. We place a uniform square grid of width $h=1/N$ on the domain and discretize (1) in a manner similar to that used in [3] for the minimal surface equation ($B=H=0$), which is related to the general procedure in [11] for linear elliptic equations.

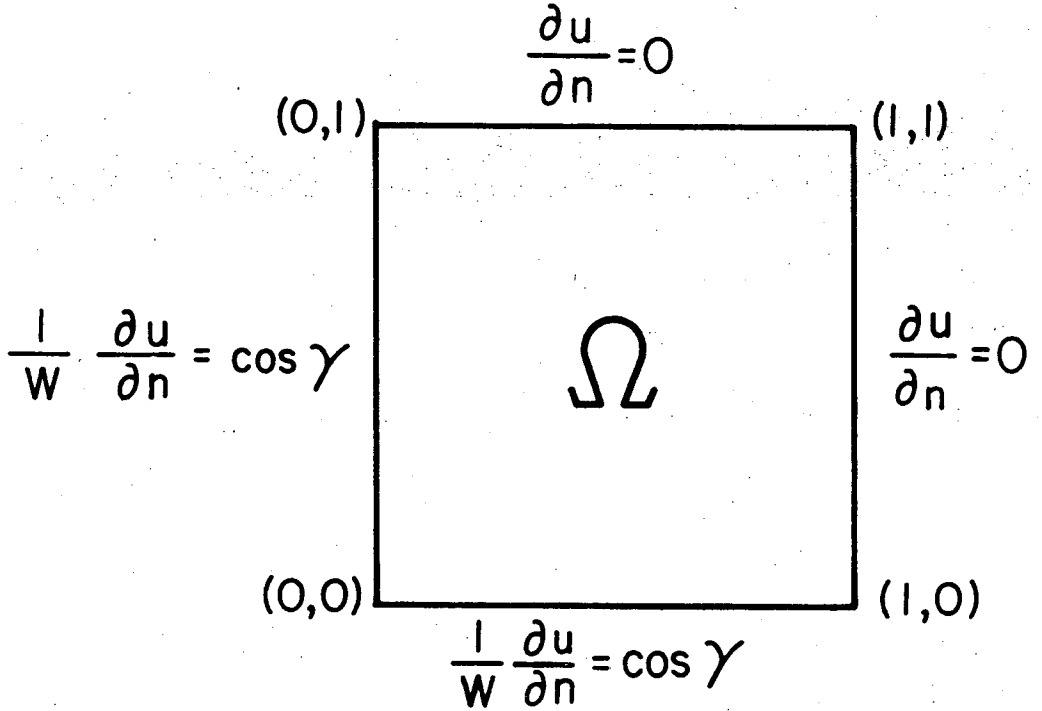

XBL 7711-2193

Fig. 1

The domain Ω for the model problem.

We write the integral form of (1), as obtained by use of Green's theorem, over a sub-domain D of Ω, which yields

$$\oint_{\partial D} \frac{1}{W}(\nabla u \cdot \underline{n})\, d\ell = \iint_{D} (Bu+2H)\, dA, \tag{4}$$

where $\underline{n}$ is the outward unit normal and ∂D is the boundary of D.

Then we place on Ω an auxiliary mesh (the dotted lines bisecting the original mesh lines in Fig. 2). We denote an h x h square bounded by the original grid lines as a cell, and we denote a rectangle bounded by auxiliary grid lines, and possibly $\partial\Omega$, as an auxiliary cell. By imposing (4) on each of the auxiliary cells and using the midpoint rule for integration, we obtain a set of (nonlinear) algebraic equations. The equation corresponding to a typical interior point $u(x,y)=u(ih,jh)=U_{i,j}$ is given by

$$\begin{aligned} f_{i,j} \equiv\ & W^{-1}_{\bar{i},\bar{j}} \left(2U_{i,j}-U_{i-1,j}-U_{i,j-1}\right) \\ & + W^{-1}_{\bar{i}+1,\bar{j}} \left(2U_{i,j}-U_{i+1,j}-U_{i,j-1}\right) \\ & + W^{-1}_{\bar{i},\bar{j}+1} \left(2U_{i,j}-U_{i-1,j}-U_{i,j+1}\right) \\ & + W^{-1}_{\bar{i}+1,\bar{j}+1} \left(2U_{i,j}-U_{i+1,j}-U_{i,j+1}\right) \\ & + 2h^2 \left(BU_{i,j}+2H\right) = 0, \end{aligned} \tag{5}$$

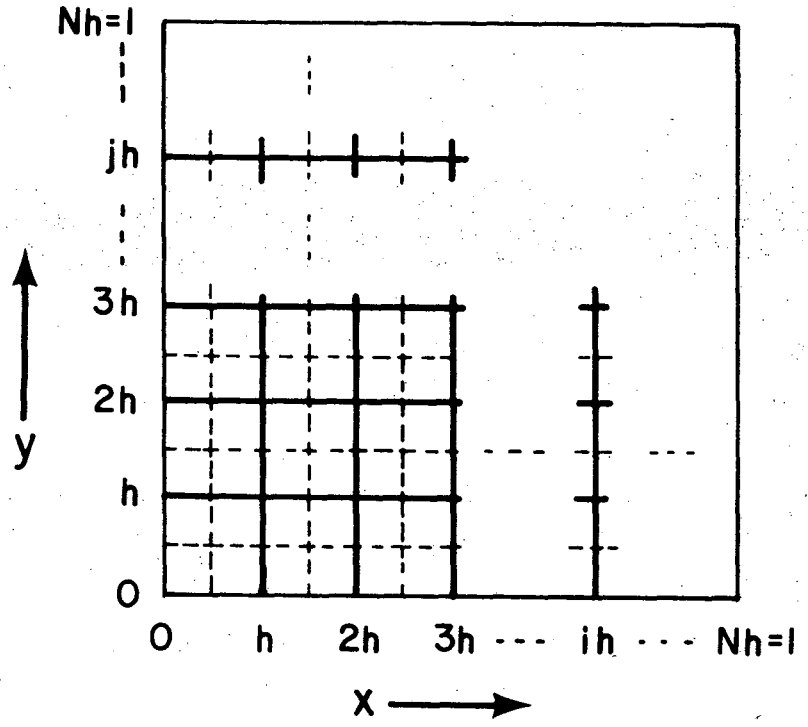

Fig. 2

The domain with the original grid and the auxiliary grid.

where $$W_{\bar{i},\bar{j}} = \left[1+\frac{1}{2}\left(\delta^2_{\bar{i},j} + \delta^2_{\bar{i},j-1} + \eta^2_{i,\bar{j}} + \eta^2_{i-1,\bar{j}}\right)\right]^{1/2},$$

with $$\delta_{\bar{i},j} = \left(U_{i,j}-U_{i-1,j}\right)/h \text{ and } \eta_{i,\bar{j}} = \left(U_{i,j}-U_{i,j-1}\right)/h.$$

Notice that the integration of (4) is performed over each auxiliary cell, and we use the approximation $\iint_D (Bu+2H)dA \doteq (BU_{i,j}+2H)\cdot(\text{area of } D)$. Note also that in the discrete equations we take W to be constant over each cell $= \left(W_{\bar{i},\bar{j}}\right.$ for the cell centered at $(i-1/2,\ j-1/2)\left.\right)$. For a boundary segment $\partial\Omega_s$ of $\partial\Omega$ we have

$$\int_{\partial\Omega_s} \frac{\nabla u\cdot\underline{n}}{W}\, d\ell = \begin{cases} \cos\gamma \cdot (\text{length of } \partial\Omega_s), & \text{if } W^{-1}\partial U/\partial n = \cos\gamma \\ 0, & \text{if } \partial u/\partial n = 0. \end{cases}$$

In the following sections, we shall discuss and compare different methods for solving the discrete equations, for the bounded and unbounded cases.

2. The Bounded Case

In this section, we investigate two methods for obtaining the solution of the discrete form of (1), (2) for the bounded case $(\alpha + \gamma \geq \pi/2)$, which for the square $(\alpha = \pi/4)$ is the case $\gamma \geq \pi/4$.

2.1. Block SOR-Newton

Here, we use the nonlinear block successive overrelaxation method investigated in [4] for solving the minimal surface equation and described in [10] as the one-step block successive overrelaxation-Newton (BSOR-Newton) method. A block SOR iteration, corresponding to a row of mesh points, is performed using a single Newton iteration to solve approximately the resulting system of nonlinear equations. We thus "solve" for one row of mesh points (see figure 2) at a time by considering the function values in that row $U_{i,j}$, $0 \leq i \leq N$, to be the only unknowns and using the latest values for all other $U_{i,j}$. If we denote by U_J, f_J the vectors $U_J = (U_{o,j}, U_{i,j}, \ldots, U_{N,j})$, $f_J = (f_{o,j}, f_{i,j}) \ldots, f_{N,j})$, and by J_{JJ} the matrix $J_{JJ} = (\partial f_{i,j}/\partial U_{k,j})$, $i,k=0,1,\ldots,N$ evaluated at the current value of $U_{i,j}$, we have the iteration

$$J_{JJ}\chi = f_J$$

$$U_J^{(\ell+1)} = U_J^{(\ell)} - \omega\chi$$

where ω is the relaxation parameter. J_{JJ} is symmetric, positive-definite, and tridiagonal, thus the solution of $J_{JJ}\chi = f_J$ can be obtained efficiently using Gauss elimination without pivoting, or Cholesky decomposition.

By differentiating (5), we obtain explicit expressions for the partial derivatives at a general interior point:

$$\frac{\partial f_{i,j}}{\partial U_{i,j}} = 2\left(W^{-1}_{\bar{i},\bar{j}} + W^{-1}_{\bar{i}+1,\bar{j}} + W^{-1}_{\bar{i},\bar{j}+1} + W^{-1}_{\bar{i}+1,\bar{j}+1} + Bh^2\right)$$

$$+ \dot{W}^{-1}_{\bar{i},\bar{j}}\left(\delta_{\bar{i},j} + \eta_{i,\bar{j}}\right)^2 + \dot{W}^{-1}_{\bar{i}+1,\bar{j}}\left(-\delta_{\bar{i}+1,j} + \eta_{i,\bar{j}}\right)^2$$

$$+ \dot{W}^{-1}_{\bar{i},\bar{j}+1}\left(\delta_{\bar{i},j} - \eta_{i,\bar{j}+1}\right)^2 + \dot{W}^{-1}_{\bar{i}+1,\bar{j}+1}\left(-\delta_{\bar{i}+1,j} + \eta_{i,\bar{j}+1}\right)^2,$$

$$\frac{\partial f_{i,j}}{\partial U_{i-1,j}} = -W^{-1}_{\bar{i},\bar{j}} - W^{-1}_{\bar{i},\bar{j}+1}$$

$$+ \dot{W}^{-1}_{\bar{i},\bar{j}}\left(\delta_{\bar{i},j} + \eta_{i,\bar{j}}\right)\left(-\delta_{\bar{i},j} + \eta_{i-1,\bar{j}}\right)$$

$$+ \dot{W}^{-1}_{\bar{i},\bar{j}+1}\left(\delta_{\bar{i},j} - \eta_{i,\bar{j}+1}\right)\left(-\delta_{\bar{i},j} - \eta_{i-1,\bar{j}+1}\right),$$

and, by symmetry, $\partial f_{i,j}/\partial U_{i+1,j} = \partial f_{i+1,j}/\partial U_{i,j}$. Here

$\dot{W}^{-1}_{\bar{i},\bar{j}} = \left[d\left(W^{-1}\right)/d|\nabla U|^2\right]_{\bar{i},\bar{j}} = -\frac{1}{2}\left(1+U_x^2+U_y^2\right)^{-3/2}$ evaluated for cell $\bar{i},\bar{j}$

(see [3][4]).

After each iteration we adjust the value of H, using (4) integrated over Ω. The left hand side yields 2 cosγ and the right hand side, after discretization, $B\bar{U} + 2H$, where $\bar{U}$ is the area-weighted average of $U_{i,j}$. The adjustment of H, which enhances the rate of convergence. corresponds to an adjustment of the volume of liquid. A final adjustment can be made, if desired, after the solution has been obtained, by moving the solution vertically to correspond to a particular liquid volume.

The convergence rate of the BSOR-Newton method depends critically on the choice of the relaxation parameter ω. Table 1 compares the number of iterations required to decrease the residual $\| f \|_2$ from its initial value of approximately 0.5 to $\leq 10^{-6}$, with zero initial approximation, $\gamma = \pi/3$, B=100, and h=1/40.

As obtained from our experiments, the estimated asymptotically optimal value of ω for the above case is 1.58. In general, it may be necessary to use a value of ω smaller than the optimal one to ensure convergence for a given initial approximation (see Tables 1 and 2). The number of iterations required for convergence can be reduced in these cases by adjusting ω towards the asymptotically optimal value as the iteration proceeds, once the approximation to U becomes sufficiently good to permit doing so. Each complete SOR sweep (for the 41 x 41 grid) takes approximately 0.055 sec. on the CDC 7600 computer (using a FORTRAN program with the FTN4 compiler, OPT = 2).

Table 1. Number of iterations required for convergence for $\gamma = \pi/3$, $B=100$, $U^{(o)} \equiv 0$ and $h=1/40$.

ω	1.2	1.3	1.4	1.5	1.6	1.7	1.8
number of iterations	>100	90	72	56	44	divergence	divergence

We have tried an initial approximation of zero for this problem, and the one of U equal to the portion of the lower hemisphere satisfying (1) and (2) for B =0 and $\gamma = \pi/4$. For these two initial approximations, the number of iterations required for convergence was essentially the same, when convergence occurred. Changing the contact angle did not affect the convergence rate substantially either, except that convergence was more rapid when γ was close to $\pi/2$.

Table 2. Number of iterations for convergence for B=100, h=1/40, and $U^{(o)} \equiv 0$.

γ \ ω	1.4	1.5	1.6
$\pi/4$	72	56	divergence
$\pi/3$	72	56	44

The size of B substantially affects the number of iterations required for convergence. The smaller B is, the larger the number of iterations required to reduce the relative error below the desired tolerance, and the stronger the dependence on ω. Table 3 compares behavior for a few values of ω for the problem $\gamma = \pi/4$, B=1 with zero initial approximation, and $\| f^{(k)} \|_2 \leq 10^{-6}$.

Table 3. Number of iterations for convergence for B=1, $\gamma = \pi/4$, h=1/40, $U^{(o)} \equiv 0$.

ω	1.5	1.8*	1.84*
number of iterations	>200	191	123

* ω was set equal to 1.5 initially to prevent divergence and was later increased progressively to the indicated value.

The slower convergence for smaller B should be expected, since for the boundary conditions (2), or those in Fig. 1, the problem becomes singular when B=0.

Judging from the experimental results, if either we have a priori knowledge of an optimal value for ω or if a scheme for improving ω is incorporated into the program, this overrelaxation method is quite efficient for larger values of B. We should add here that this method works also for the case B=0, for which a closed-form solution is known. We discuss further experimental results for the behavior of the BSOR-Newton method in Sec. 2.3, where a comparison is made with results for the method discussed in the following section.

2.2. Hybrid conjugate gradient method

In this section, the conjugate gradient method is combined with a fast Helmholtz solver to obtain iteratively the solution to the discrete

form of (1) and (2). This method proceeds as follows (see [8]):

(i) Given an initial approximation $U^{(o)}$ ($U^{(o)}$ is a vector of length $(N+1)^2$). Arbitrarily define $p^{(-1)}$. For k = 0, 1, 2, ...

(ii) Compute

$$f^{(k)} = f_{ij}(U^{(k)})$$

and solve $Mz^{(k)} = -f^{(k)}$.

(iii) Compute the search direction

$$p^{(k)} = z^{(k)} + \beta_k p^{(k-1)},$$

$$\text{where } \beta k = \frac{\left(f^{(k+1)}, z^{(k+1)}\right)}{\left(f^{(k)}, z^{(k)}\right)} \quad k \neq 0, m, 2m, 3m, \ldots$$

$$\beta_0 = \beta_m = \beta_{2m} = \ldots = 0.$$

(iv) Compute the new approximation

$$U^{(k+1)} = U^{(k)} + \alpha_k p^{(k)},$$

$$\text{where } \alpha_k = -\frac{\left(f^{(k)}, z^{(k)}\right)}{\left(p^{(k)}, Jp^{(k)}\right)}$$

and J is the Jacobian matrix $\left(\partial f_{i,j}/\partial U_{r,s}\right)$ evaluated at $U^{(k)}$. In our experiments we choose the restart parameter to be m = 9, as in [8], and we continue the iteration until $\|f^{(k)}\|_2 \leq$ EPS, where EPS is the desired tolerance.

We choose the matrix M in step (ii) to be one that approximates J in some sense and for which a fast-direct method can be used to solve $Mz^{(k)} = -f^{(k)}$. Our choice is the discrete Helmholtz operator scaled by a

diagonal matrix (see [8]). Specifically, $M = D^{1/2}(-2\Delta_h+KI)D^{1/2}$, where D is a diagonal matrix whose entries are $(\partial f_{i,j}/\partial U_{i,j}-2Bh^2)/[2 \text{ diag } (-\Delta_h)]$, and $2\Delta_h$ is twice the discrete five-point Laplace operator on a mesh of width h, obtained by setting $W \equiv 1$ in the discrete form of (1), (2). We make the choice $K = 2Bh^2$, so that M is identical to the discrete form of (1), (2) when $W \equiv 1$.

To solve $Mz^{(k)} = -f^{(k)}$ we follow steps a to c below:

(a) Compute $-D^{-1/2}f^{(k)}$.

(b) Use a fast solver to find χ, where

$$\left(-2\Delta_h + 2Bh^2\right)\chi = -D^{-1/2}f^{(k)}.$$

(c) Compute $z^{(k)} = D^{-1/2}\chi$.

The multiplication of $Jp^{(k)}$ in the calculation of α_k in step (iv) of the algorithm is carried out utilizing fully the sparsity of J. Since J is block tridiagonal and each block is itself tridiagonal the multiplication takes less than $9(N+1)^2$ operations.

In the table below, we list the number of iterations to obtain $\left\|f^{(k)}\right\|_2 \leq$ EPS for different γ and B with h = 1/40, EPS = 10^{-6}, and $H \equiv 1$.

Table 4. Number of iterations required for convergence for h = 1/40 and $U^{(o)} \equiv 0$.

γ \ B	100	1	0.1	0.01
$\pi/4$	13	22	28	40
$\pi/3$	8	10	10	10

Each iteration takes approximately .139 sec., which includes .073 sec. for the fast solver, except for the first iteration, which requires 0.183 sec. including preprocessing. The program GMA (with parameter K=2) [2] was used to obtain the fast solution of Helmholtz's equation in our experiments. Notice that the dependence on the value of γ in Table 4 is much stronger than it is for the BSOR-Newton method. The smaller the angle, the more nonlinear the problem, and the more iterations required because M is less good an approximation to J and hence to f. Here, the value of B also influences the number of iterations required for convergence, more so in the case $\gamma = \pi/4$, for which W becomes very large near the corner (0,0). The singular case B=0 can also be handled by this method when used with an appropriate fast solver.

2.3. Comparisons

We summarize the data from some of our experiments in the following tables. In all cases the initial approximation $U^{(o)} \equiv 0$ is used and the number of iterations given are those required to obtain a residual $\|f^{(k)}\|_2 \leq \text{EPS}$.

It appears, from the data in Tables 5 and 6, that the hybrid conjugate gradient method performs consistently better in terms of computer time for the model problem than does the block overrelaxation-Newton method. The conjugate gradient method has the further advantage of not requiring the estimation of an acceleration parameter such as ω (the dependence on the value of the restart parameter m is not as significant), and it is

Table 5. Number of iterations (CPU seconds) for the BSOR-Newton iteration

h	B	γ	Estimated best ω	ω for first 20 iterations	ω after 20 iterations	EPS= 10^{-3}	10^{-4}	10^{-5}	10^{-6}
$\frac{1}{40}$	100	π/3	1.58	1.6	1.6	21(1.13)	29(1.56)	37(1.99)	44(2.36)
	100	π/4	1.59	1.5	1.55	25(1.34)	34(1.83)	43(2.31)	51(2.74)
	1	π/3	1.84	1.5	1.84	79(4.24)	98(5.26)	116(6.22)	>120(6.44)
	1	π/4	1.84	1.5	1.84	77(4.13)	90(4.83)	107(5.74)	>120(6.44)
	.01	π/3	1.85	1.5	1.8	116(6.22)	>120(6.44)		
	.01	π/4	1.85	1.5	1.8	118(6.33)	>120(6.44)		
$\frac{1}{20}$	100	π/3	1.52	1.2	1.5	15(.21)	20(.28)	24(.34)	27(.38)
	100	π/4	1.52	1.2	1.5	15(.21)	22(.31)	24(.34)	27(.38)
	1	π/3	1.71	1.5	1.7	46(.64)	56(.78)	66(.92)	76(1.06)
	1	π/4	1.71	1.5	1.7	46(.64)	55(.77)	65(.91)	75(1.05)
	.01	π/3	1.81	1.5	1.8	48(.67)	58(.81)	66(.92)	79(1.11)
	.01	π/4	1.82	1.5	1.8	49(.69)	58(.81)	67(.94)	79(1.11)

TABLE 6. Number of iterations (CPU seconds) for the conjugate gradient iteration

h	B	γ	EPS= 10^{-3}	10^{-4}	10^{-5}	10^{-6}
	100	$\pi/3$	4(.60)	5(.74)	6(.88)	8(1.16)
	100	$\pi/4$	6(.79)	8(1.16)	10(1.44)	13(1.90)
	1	$\pi/3$	5(.74)	7(1.02)	8(1.16)	10(1.44)
$\frac{1}{40}$	1	$\pi/4$	13(1.90)	15(2.18)	18(2.59)	22(3.19)
	.01	$\pi/3$	5(.74)	6(.88)	8(1.16)	10(1.44)
	.01	$\pi/4$	15(2.18)	29(4.16)	34(4.91)	40(5.74)
	100	$\pi/3$	4(.14)	5(.17)	6(.21)	7(.24)
	100	$\pi/4$	5(.17)	6(.21)	7(.24)	9(.30)
	1	$\pi/3$	5(.17)	7(.24)	8(.27)	9(.30)
$\frac{1}{20}$	1	$\pi/4$	10(.34)	14(.48)	16(.54)	19(.64)
	.01	$\pi/3$	5(.17)	6(.21)	8(.27)	9(.30)
	.01	$\pi/4$	13(.44)	22(.74)	25(.84)	35(1.18)

less sensitive to the initial approximation, although it does require more computer storage than is required for the BSOR-Newton method [8]. For nonrectangular domains the conjugate gradient method would lose some of its competitive advantage of speed since more computer time is required by fast-direct methods in this case for the solution of the Helmholtz equation. See [8] for other possible choices for M and for comparisons of the conjugate gradient method with the BSOR-Newton method for the case B = H = 0 with boundary conditions for which the problem is not singular.

In order to estimate the discretization error, the numerical solution for B=0, $\gamma = \pi/4$, h = 1/20 was compared with the known closed-form solution. We found the relative error of the computed solution in the infinity norm to be less than about 1/2% everywhere beyond 3 grid points from the corner, 18% right at the corner, and 1 to 4% in between. The relative difference between the computed solutions on the grids for h = 1/40 and h = 1/20 was about 2% in the infinity norm for this case.

3. The unbounded case

As pointed out in Sec. 1, there is a critical contact angle γ_o, which is $\pi/4$ for our model problem, such that the solution is unbounded at the corner of the cylinder cross section for all $\gamma < \gamma_o$. The asymptotic form of the solution in a neighborhood of the corner is given by (3). If $\gamma < \gamma_o$, we use this asymptotic solution in conjunction with discrete methods away from the corner to solve our problem.

We investigate two methods that use different discretization procedures over the portion of the domain away from the corner. In the first method, a neighborhood of the corner is deleted entirely from the domain to be discretized. In the second, the asymptotic solution is extended into part of this domain. We consider, as in the previous section, only the model problem of a square on which has been placed a uniform square mesh.

3.1. Method A

Here we assume that the asymptotic behavior (3) holds from the vertex of the corner with the singularity up to one or several grid points away. We term this portion of the domain the asymptotic domain and the remaining portion the numerical domain (see figure 3).

A natural way to obtain the numerical domain is to cut along a level curve of the asymptotic solution. The analytical solution in this domain then can provide an upper bound on the solution u of (1),(2) [9]. Although the level curves of the asymptotic solution are circular arcs, the limitations of our experimental computer program require us to approximate such an arc by a straight line passing through mesh points and making an angle of 45° with the edges of the square. Thus, we solve equations (1) and (2) numerically in the domain shown in figure 4.

The boundary conditions of the previous section apply at all boundary points, except those on Γ, where we use a normal-derivative matching condition obtained by differentiating (3). After solving the resulting problem in the numerical domain, we can obtain a value for v - u in the

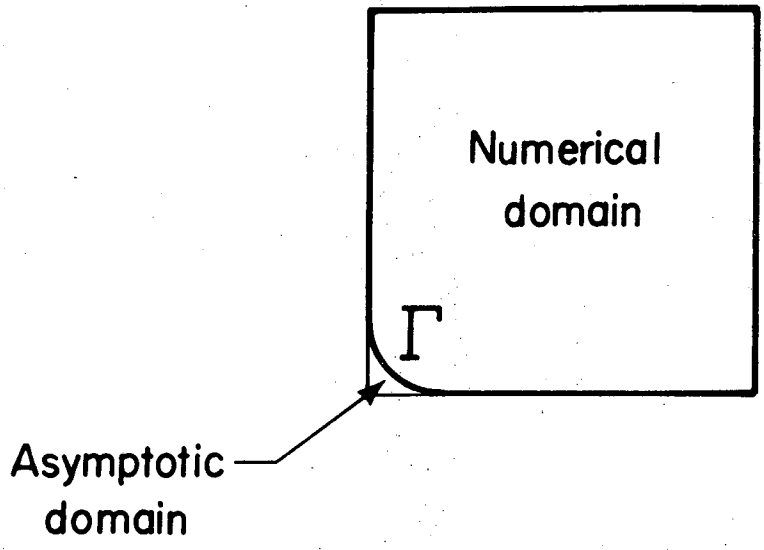

Fig. 3

Division of the domain for Method A.

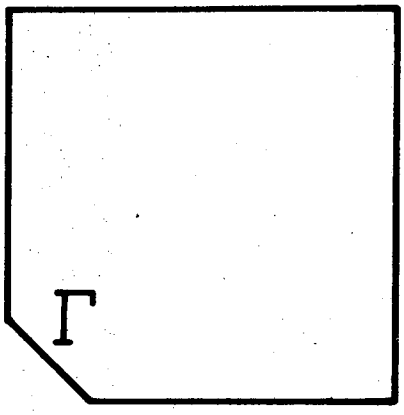

Fig. 4

The numerical domain for the test problem.

XBL7711-2188

asymptotic domain by matching at one (or more) points of Γ. In this way, we obtain an approximation to the solution over the entire domain Ω.

We use the same discrete equation(5) at a general interior point of the numerical domain as in Sec. 2.1. On Γ, the discrete equation at a general point is (see figure 5)

$$f_{i,j} = W^{-1}_{\bar{i}+1,\bar{j}+1}\left(2U_{i,j} - U_{i+1,j} - U_{i,j+1}\right) - W^{-1}_{\bar{i},\bar{j}+1}\left(U_{i,j+1} - U_{i,j}\right)$$

$$- W^{-1}_{\bar{i}+1,\bar{j}}\left(U_{i+1,j} - U_{i,j}\right)$$

$$- 2\int_{\Gamma_i} \frac{1}{W}\frac{\partial U}{\partial n}\, d\ell + h^2\left(BU_{i,j} + 2K\right) = 0,$$

where

$$W_{\bar{i},\bar{j}+1} = \left[1 + \left(U_{i,j+1} - U_{i-1,\,j+1}\right)^2/h^2 + \left(U_{i,j+1} - U_{i,j}\right)^2/h^2\right]^{1/2},$$

$$W_{\bar{i}+1,\bar{j}} = \left[1 + \left(U_{i+1,j} - U_{i,j}\right)^2/h^2 + \left(U_{i+1,j} - U_{i+1,j-1}\right)^2/h^2\right]^{1/2},$$

and $\int_{\Gamma_i} \frac{1}{W} \frac{\partial U}{\partial n}\, d\ell$ is evaluated by Simpson's rule using the directional derivative from (3) for the values of $W^{-1}\partial v/\partial n$,

$$\left.\frac{1}{W}\frac{\partial U}{\partial n}\right|_{\Gamma} = \frac{-a_1(x+y) + a_2(y-x)}{\left[2\left(x^2+y^2\right)\left(1+a_1^2+a_2^2\right)\right]^{1/2}}\,, \tag{6}$$

where $a_1 = -\left(\cos\theta - \left[\kappa^2 - \sin^2\theta\right]^{1/2}\right)/\left(\kappa B \rho^2\right)$

$$a_2 = \left(\sin\theta\cos\theta\left[\kappa^2 - \sin^2\theta\right]^{-1/2} - \sin\theta\right)/\left(\kappa B \rho^2\right)$$

$(\theta, \kappa, B, \rho$ as defined in (3)).

The discrete equation for points one mesh interval away from Γ in the interior of the numerical domain is the same as (5), except that for (i, j) on Γ, $W_{\bar{i},\bar{j}}$ is given by $W_{\bar{i},\bar{j}} =$

$$\left(1 + \left(U_{i,j} - U_{i,j-1}\right)^2/h^2 + \left(U_{i,j} - U_{i-1,j}\right)^2/h^2\right)^{1/2}.$$

We consider only the BSOR-Newton method for solving the discretized equations in the numerical domain. General purpose programs for solving the discrete Helmholtz equation are being developed and were not available for use with the conjugate gradient method during our study. These programs require, in general, more computer time than ones for a rectangular domain.

The determination of how far into the domain Γ should be placed for optimal accuracy poses an essential difficulty for the method: If

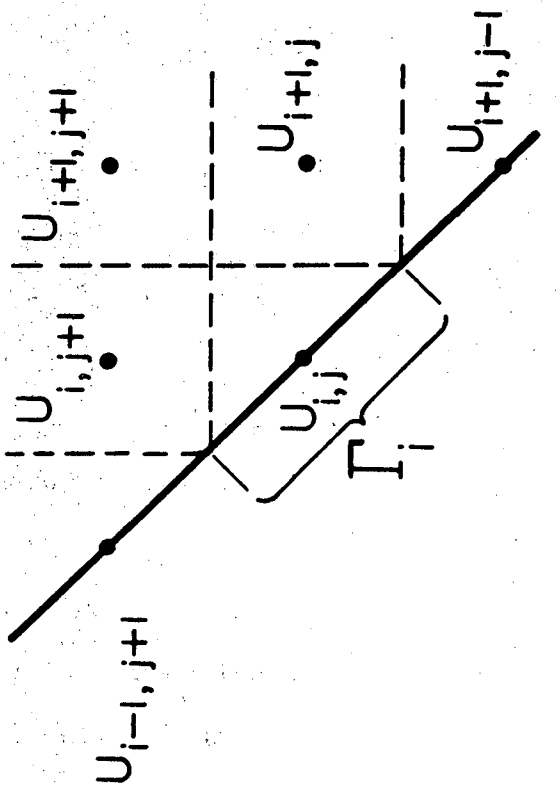

XBL 7711-2191

Fig. 5

The boundary points of Γ.

Γ is too far into the domain, the boundary condition obtained from the asymptotic representation on Γ will be inaccurate; if Γ is too close to the corner, the discretization in the numerical domain near Γ may not be able to represent well the steepness of the solution. Considering these two alternatives, it appears that it is better to put Γ close to the corner, because one can, in principle, always refine the mesh locally or use higher-order or other methods to handle the steepness of the solution, while errors committed by pushing Γ too far into the domain cannot be compensated for easily.

In our numerical experiments, we choose Γ to be sufficiently close to the corner so that at p, the midpoint of Γ, $W^{-1}\partial\nu/\partial n \geq 0.999 \doteq \cos^{-1}2.5°$. We solve the resulting problem on the numerical domain with a mesh size h of 1/40 and 1/80, to give an indication of the discretization error for the particular choice of Γ. We also solve problems for nearby choices of Γ to determine the sensitivity to the positioning of Γ.

Of course, the matching conditions (6) on Γ may not be accurate. Although the difference between u and the asymptotic solution ν is bounded by a constant as the corner is approached, the difference between their derivatives may be large. If Γ is chosen to be an actual level curve of ν, close enough to the vertex so that $|\nabla\nu|$ is large and $W^{-1}\partial\nu/\partial n$ is essentially 1 there, then $|\nabla u|$ would also be large and choosing $W^{-1}\partial u/\partial n$ to be essentially 1 along Γ should then be sufficiently

accurate to be in keeping with the discretization errors in the interior. However, along the straight-line approximation to the level curve required by our test program, $W^{-1}\partial v/\partial n$ can vary appreciably, and attempting to match to $W^{-1}\partial u/\partial n$ as in (6) might lead to errors. Our goal is to obtain from our experimental program not necessarily solutions of the highest accuracy but rather an indication of the feasibility of our use of the asymptotic solution (3) near the corner singularity in conjunction with a discrete method elsewhere.

We give here a summary of some of the typical behavior found in our numerical experiments.

For the case $\gamma = 0°$, $B = 1$, and Γ at the position where $W^{-1}\partial v/\partial n|_p \doteq 0.999$ (i.e., Γ is on the 17th grid point of the first row in an 81×81 mesh, or the 9th grid point of the first row in a 41×41 mesh), moving Γ one grid point in the 81×81 mesh produces less than .1% relative difference in the solution in the interior 90% of the domain, between .1% and 1% relative difference in a band closer to Γ covering about 7% of the domain, and between 1% and 3.5% for the points in the immediate neighborhood of Γ. The relative difference is correspondingly about twice as much in the 41×41 case when Γ is moved by one mesh point. The relative difference in the solution resulting from refining the mesh from 1/40 to 1/80, keeping Γ fixed, is less than 0.2% over the interior 50% of the domain, between 0.2% and 1% over 30% of the domain, between 1% and 5% over 10% of the domain, and between 5% and 15% on the points in the immediate neighborhood of Γ.

For $\gamma = 30°$, $B = 1$, and $W^{-1}\partial v/\partial n|_p \doteq 0.999$, the relative differences are about one-fourth of those of the above experiments for $\gamma = 0°$. Less sensitivity is to be expected because the solution surface is generally not as steep in this case. For similar reasons, the case for $\gamma = 0°$, $B = 10$, $W^{-1}\partial v/\partial n|_p \doteq 0.999$, has about only half of the relative differences found for the case $\gamma = 0°$, $B = 1$.

If we choose Γ so that $W^{-1}\partial v/\partial n|_p \doteq 0.9999$, then the relative differences from refining the mesh were found to be two to three times as large as they were for placing Γ at a position for which $W^{-1}\partial v/\partial n|_p \doteq 0.999$.

Based on the above information, we choose Γ so that $W^{-1}\partial v/\partial n|_p \doteq 0.999$ for most of our experiments.

For the case of $\gamma = 0°$, $B = 1$, the solution height in the numerical domain was found to be $U|_p \doteq 1.46$ for the 81×81 grid. We compare solution heights obtained from placing Γ on the 9th grid point on the first row (in this case, $W^{-1}\partial v/\partial n|_p \doteq 0.9999$) and placing Γ on the 17th grid point on the first row (in this case, $W^{-1}\partial v/\partial n|_p \doteq 0.999$) on a 81×81 grid. Although rather large relative differences exist for points close to Γ, we observe that over 75% of the domain less than a 1% change occurs. This indicates that the solution over a large portion of the domain is rather insensitive to where Γ is placed. As mentioned previously, over the same large portion, refining the mesh from 1/40 to 1/80 also produces only minor changes. Thus, for that portion of the domain, a medium size mesh (say, $h = 1/40$) seems sufficient to produce acceptably

accurate results. We observe also that for fixed Γ the numerical solution appears to be converging as h tends to zero through the different mesh sizes.

For the unbounded case, the convergence of the BSOR-Newton method is even more sensitive to changes of ω than for the bounded case, especially for $\gamma = 0°$. For $U^{(o)} \equiv 0$, one must begin the iteration with ω close to 1 to prevent divergence, and then quickly (within 20 iterations, say) increase ω toward the estimated optimal value in order to obtain an acceptably rapid convergence rate. Overestimating ω essentially always leads to divergence. For $\gamma = 0°$, the observed optimal values of ω found experimentally are listed in Table 7.

Table 7. Observed optimal ω for $\gamma = 0°$.

h \ B	1	10	100
1/20	1.70	1.61	1.33
1/40	1.84	1.78	1.50
1/80	1.92	1.88	not available

The optimal values of ω for $\gamma = 30°$ are about the same as for $\gamma = 0°$. One can see from Table 7 that both the grid size and value of B influence the value of the optimal ω.

Table 8 summarizes our experimental results for a range of values of γ, B, and h. The number of iterations

TABLE 8. Number of iterations (CPU seconds) for method A

γ	B	h	Γ^*	Initial† approx.	ω starting	ω after 20 steps	ω_{opt} (estimated)	DEL = 10^{-3}	10^{-4}	10^{-5}	10^{-6}
0	1	$\frac{1}{20}$	4	S	1.5	1.69	1.70	31(.46)	42(.63)	51(.76)	61(.91)
0	1	$\frac{1}{40}$	8	S	1.79	1.84	1.84	37(2.04)	56(3.08)	71(3.91)	85(4.68)
0	1	$\frac{1}{80}$	16	S	1.79	1.84**	1.92	70(16.1)	112(25.76)	170(39.10)	
0	10	$\frac{1}{20}$	1	0	1.5	1.59	1.61	24(.35)	33(.49)	41(.61)	48(.72)
0	10	$\frac{1}{40}$	1	0	1.55	1.75	1.78	46(2.53)	64(3.53)	81(4.46)	97(5.34)
0	10	$\frac{1}{80}$	4	0	1.55	1.79††	1.89	90(20.70)	141(32.43)	178(40.94)	
$\frac{\pi}{6}$	1	$\frac{1}{20}$	3	S	1.5	1.69	1.71	24(.36)	38(.57)	48(.71)	59(.88)
$\frac{\pi}{6}$	1	$\frac{1}{40}$	6	S	1.79	1.84	1.84	26(1.43)	50(2.75)	68(3.74)	84(4.62)
$\frac{\pi}{6}$	10	$\frac{1}{20}$	1	0	1.5	1.59	1.61	25(.37)	34(.51)	42(.63)	50(.75)
$\frac{\pi}{6}$	10	$\frac{1}{40}$	1	0	1.55	1.75	1.78	48(2.64)	66(3.64)	84(4.63)	102(5.62)

*The number of grid intervals from the corner at which Γ meets an edge of Ω.

**ω = 1.9 after 100 iterations.

†0 - identically zero; S-portion of a sphere (i.e. exact solution for B=0, $\gamma=\pi/4$).

††ω = 1.87 after 100 iterations.

given in Table 8 are those required for $\|U^{(k)}-U^{(k-1)}\|_2 / \|U^{(k)}\|_2 \leq$ DEL.

A major difficulty for this method is the representation of the steep gradients of the solution in the numerical domain near Γ. In the next section, we investigate the possibility of handling this difficulty by overlapping a portion of the numerical with the asymptotic domain.

3.2. Method B

Here we investigate the possibility of improving the previous method by overlapping the asymptotic and numerical solutions over part of the domain. We divide the entire domain into the three regions shown in Figure 6. Region I is a small portion of the domain near the corner in which we assume that the asymptotic behavior (3) holds. Region III, including boundary 2 in Figure 6, is the purely numerical domain, in which we assume that the solution u is not too steep and can be computed accurately with the discretization used previously. The region between is Region II, where we couple the asymptotic and numerical solutions under the assumption that u and v differ there by a lower-order quantity that is not steep and thus can be computed more accurately with a discretization than can either u or v. The staircase-shaped domain boundaries are used rather than the 45° lines of Method A to approximate level curves because the limitations of our study permitted us to use only those boundaries that were simplest to include in the computer program.

Let u be the solution to (1) and (2), then in Region I and II we

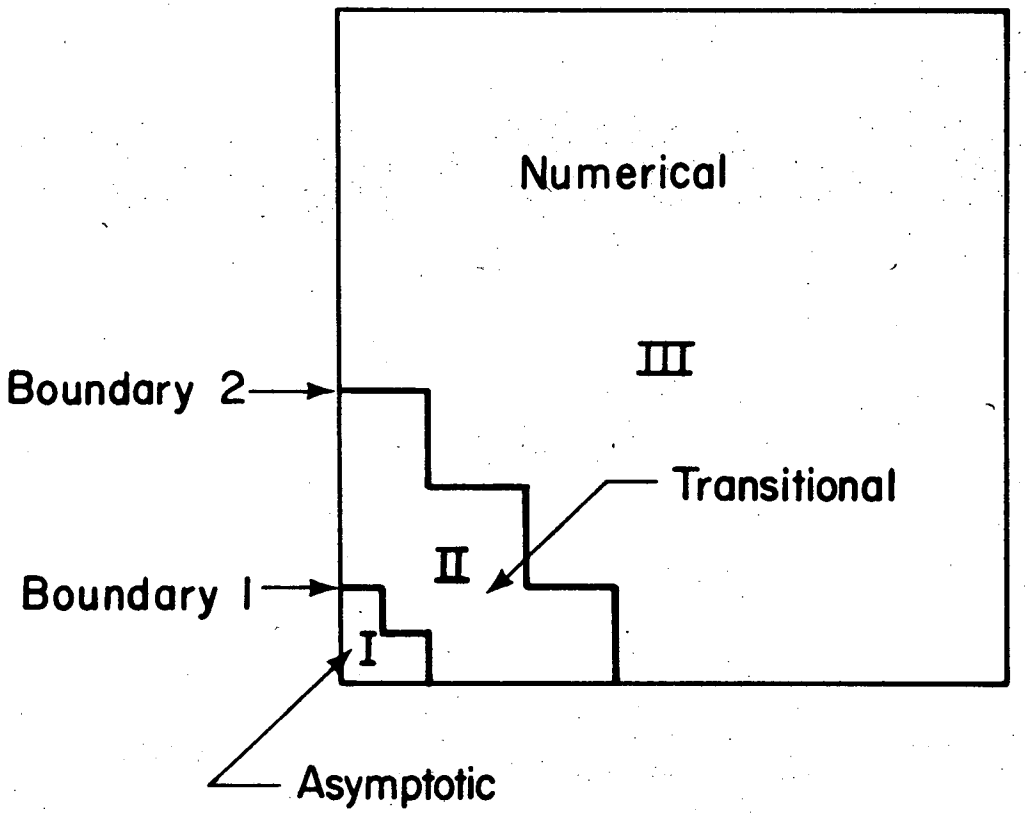

XBL 7711-2189

Fig. 6

The three regions for Method B.

write $u = \nu + \varepsilon$, where ν is given by the asymptotic expression (3) and $|\varepsilon|$ is bounded by a constant. Over Region II, we consider $\varepsilon(x,y) = u(x,y) - \nu(x,y)$ and we derive discrete equations for $\varepsilon(x,y)$ involving the known quantity ν, keeping only the first-order terms in ε/ν and in the derivatives of ε divided by those of ν. Over Region I, we take $\varepsilon = \varepsilon_o$, as in Method A, where ε_o and its derivatives are negligible compared with ν and its derivatives.

In Region II, the left hand side of (4) becomes

$$\int_{\partial D} \frac{(\nu+\varepsilon)_n}{\left[1+(\nu_x+\varepsilon_x)^2+(\nu_y+\varepsilon_y)^2\right]^{1/2}}\, d\ell$$

$$= \int_{\partial D} \frac{(\nu+\varepsilon)_n}{\left[1+\nu_x{}^2+\nu_y{}^2\right]^{1/2}} \left[1 + \frac{-\nu_x\varepsilon_x - \nu_y\varepsilon_y}{\left(1+\nu_x{}^2+\nu_y{}^2\right)} + O\left(\frac{\varepsilon_x{}^2+\varepsilon_y{}^2}{\nu_x{}^2+\nu_y{}^2}\right)\right] d\ell. \qquad (7)$$

When we perform the integration along a direction parallel to y-axis, then the normal direction in (7) is parallel to the x-axis, and the right-hand side of (7) becomes (see figure 7)

$$\int_C \frac{\nu_x\, d\ell}{\left[1+\nu_x{}^2+\nu_y{}^2\right]^{1/2}} + \int_C \varepsilon_x \frac{1+\nu_y{}^2}{\left[1+\nu_x{}^2+\nu_y{}^2\right]^{3/2}}\, d\ell - \int_C \varepsilon_y \frac{\nu_x\nu_y}{\left[1+\nu_x{}^2+\nu_y{}^2\right]^{3/2}}\, d\ell \qquad (7a)$$

+ higher order terms.

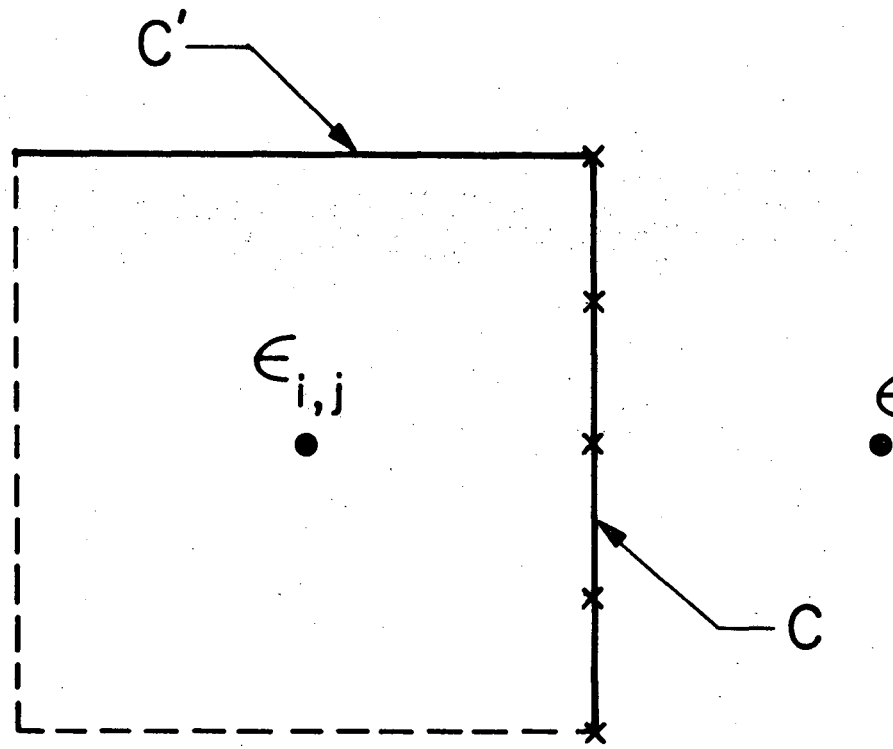

Fig. 7

Integration path on an auxiliary mesh cell boundary

If the normal direction $\underline{n}$ is parallel to the y-axis, as along C', then the right-hand side of (6) becomes

$$\int_{C'} \frac{\nu_y \, d\ell}{\left[1+\nu_x^2+\nu_y^2\right]^{1/2}} + \int_{C'} \varepsilon_y \frac{1+\nu_x^2}{\left[1+\nu_x^2+\nu_y^2\right]^{3/2}} \, d\ell - \int_{C'} \frac{\nu_x \nu_y}{\left[1+\nu_x^2+\nu_y^2\right]^{3/2}} \, d\ell \tag{7b}$$

$$+ \text{ higher order terms.}$$

To form discrete equations for $\varepsilon_{i,j}$, we evaluate (7a) along C, for example, by using Simpson's rule with the five indicated node points for computing the three integrals involving ν, with ε_x replaced by $(\varepsilon_{i+1,j} - \varepsilon_{i,j})/h$ and ε_y replaced by $(\varepsilon_{i,j-1} - \varepsilon_{i,j} + \varepsilon_{i+1,j+1} - \varepsilon_{i+1,j})/2h$ for the upper half of C and by $(\varepsilon_{i,j} - \varepsilon_{i,j-1} + \varepsilon_{i+1,j} - \varepsilon_{i+1,j-1})/2h$ for the lower half of C. If we then ignore terms that contain powers greater than one of ε/ν and of the ratio of their derivatives, we obtain a system of linear equations for $\varepsilon_{i,j}$. The associated matrix is symmetric and banded.

3.2.1. The iteration

In solving the discrete equations in Region II, the boundary condition on boundary 1 is obtained from the directional derivative of the asymptotic formula (3), and the boundary condition at each iteration for boundary 2 is obtained by keeping the value of u fixed at its Region III value. We use the IMSL subroutine LEQT1B, designed to solve banded systems, to obtain the solution. Note that for the different boundary

conditions on boundary 2 arising from each iteration, only the right hand side of the system to be solved in Region II needs to be changed. Therefore, it is necessary to perform the associated triangular decomposition only for the first iteration.

The method of solution for Region III is the BSOR-Newton method of the previous sections. The boundary condition on boundary 2 is that of keeping the value of U(i.e. ε) fixed at its value obtained previously in Region II. Afterwards, we adjust the value of H in the same way as before, using the boundary of Region III as the contour for (3).

Each iteration thus consists of solving for ε in Region II followed by solving for U in Region III and then adjusting H.

3.2.2. Experimental Results

We have experimented with this method for $\gamma = 0°$, B = 1 and B = 10 on a 41 × 41 grid. We took boundary 1 to intersect the edge of the square one grid point from the corner, and boundary 2 to intersect the edge at the 10th grid point for B = 1 and the 4th grid point for B = 10. We found the solutions generally insensitive to these boundaries being moved by one or two mesh intervals. The time required for convergence was about three times greater than for Method A.

Of importance is the observation, that in our experiments the value of $|\nabla\varepsilon|$ obtained was not necessarily small compared with that of $|\nabla\nu|$. In fact, $|\nabla\varepsilon|$ was almost half of $|\nabla\nu|$ for most points in Region II, including the points close to the vertex. Thus the assumption, on which the numerical scheme in Region II is based, that $|\nabla\varepsilon| \,/\, |\nabla\nu|$ is small does not hold even though $|\varepsilon| \,/\, |\nu| \to 0$ as the vertex is approached.

3.3. Conclusion

Since the results from Method B indicate that the assumption on which it is based does not generally hold, we conclude that Method B is not a suitable technique for improving Method A for this problem. The experimental results for Method A for the 21 × 21, 41 × 41, 81 × 81 grids, for a fixed position of Γ indicate convergence of the numerical solution as h(the mesh size) → 0. In addition, the values of U on the bulk of the domain change very little as the mesh is refined, indicating that reasonable accuracy can be obtained away from the corner even for the coarser grids.

From the experimental data, it appears that taking Γ to be the line on which the value of ν_n/W at the midpoint is about 0.999 is reasonably satisfactory. Moving Γ one or two mesh intervals produces less than 0.5% relative difference in the numerical solution over 90% of the grid points. As for the points close to Γ, one should consider using a finer mesh or higher-order discretization than in the rest of the domain and taking Γ to be a level curve of the asymptotic solution with an irregular mesh nearby. These matters are considered further in a related study [1].

In Figures 9 to 18, we present graphical computer output depicting perspective views with contours for some of the numerical solutions

that were obtained with the methods of Section 2 for the bounded case and with Method A for the unbounded case. The perspective views displayed are those indicated in figure 8. The height contours are drawn at intervals of 0.1, measured from the center (1,1) where the height is taken to be zero.

Solution surfaces for B=1 are depicted in figure 9 for $\gamma=60°$ (a bounded case) and in figures 10 to 13 for $\gamma=30°$ and $\gamma=0°$ (unbounded cases). Those for B=10 are depicted in figure 14 for $\gamma=60°$ and figures 15 to 18 for $\gamma=30°$ and $\gamma=0°$. All perspective views are at an inclination angle of 20° and a viewpoint distance of 100 units.

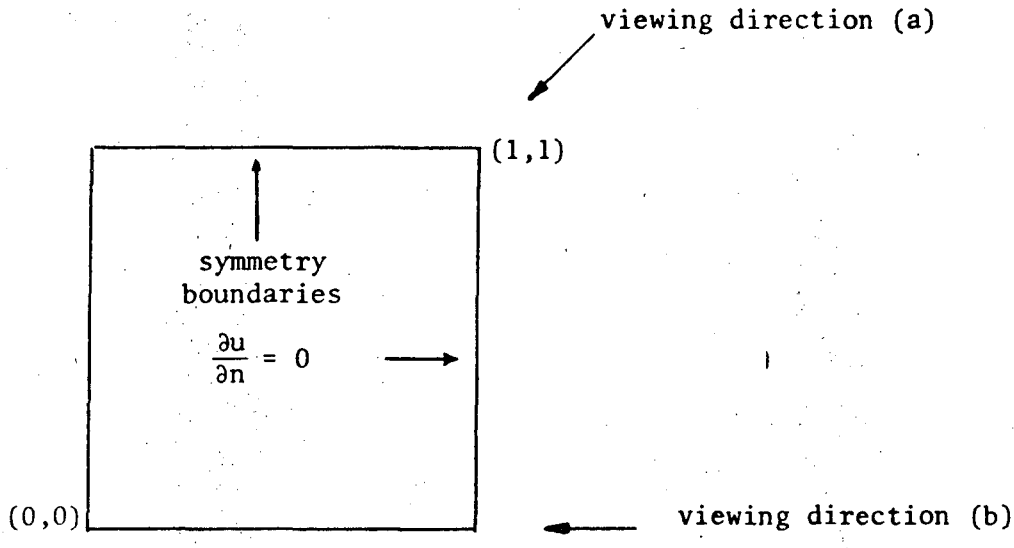

Figure 8

Test problem domain showing perspective viewing directions.

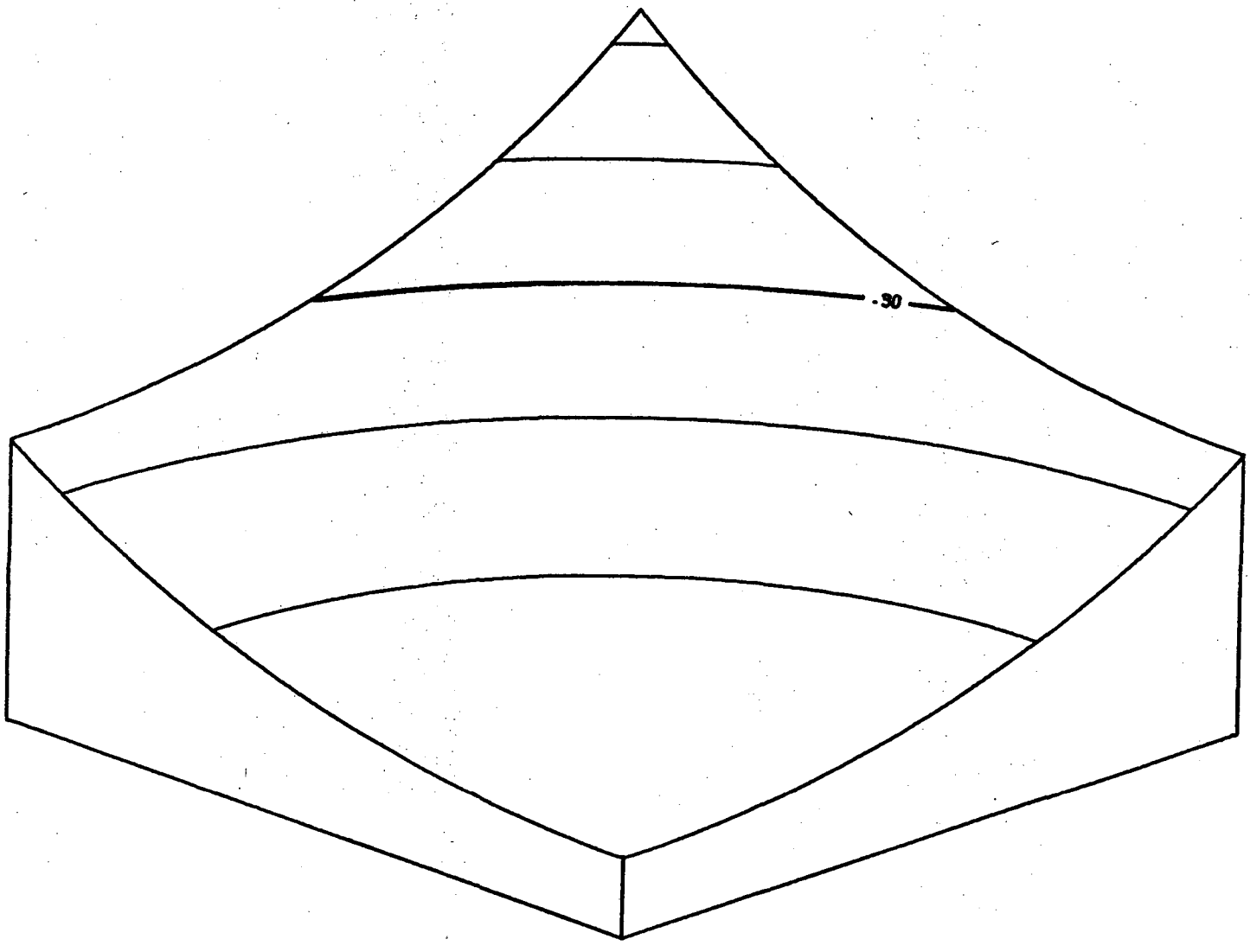

Figure 9

Perspective view for B = 1 from direction (a), $\gamma = 60^{o}$.

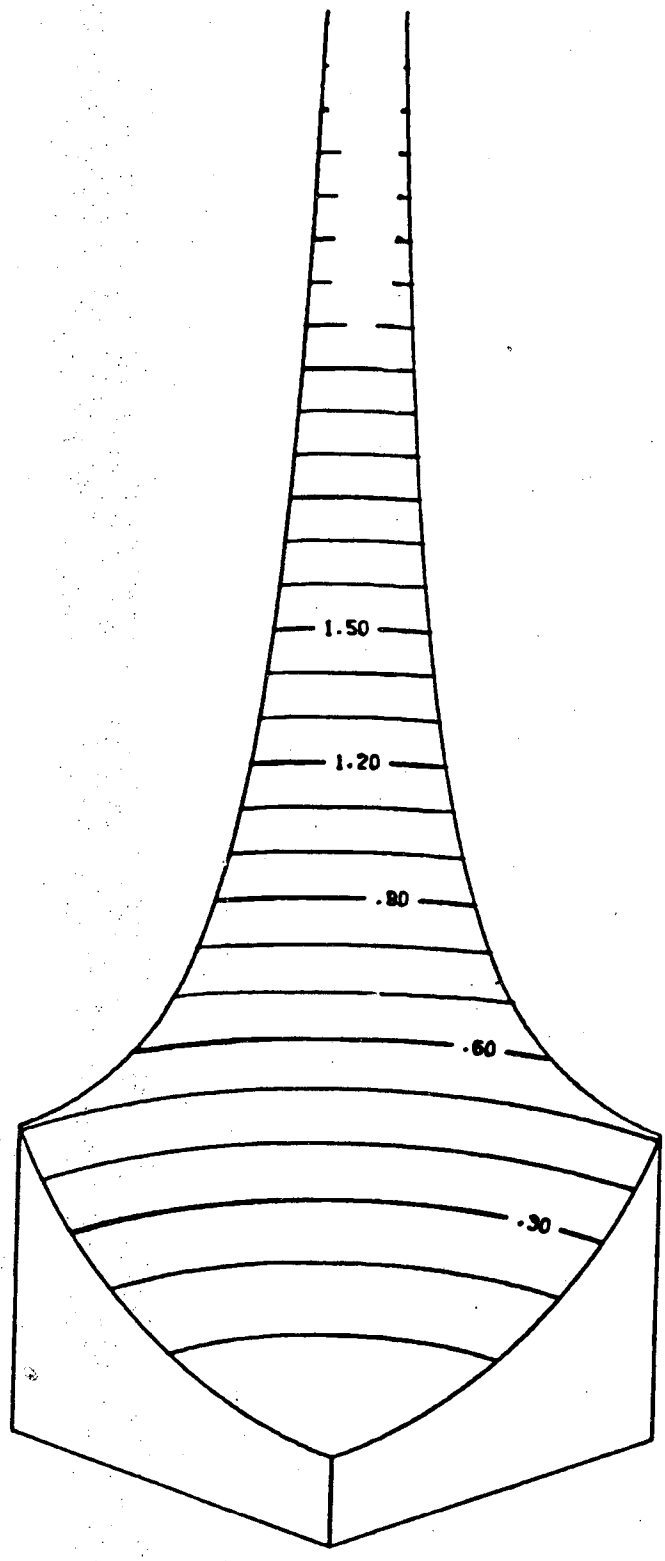

Figure 10. Perspective view for B = 1 from direction (a), $\gamma = 30°$.

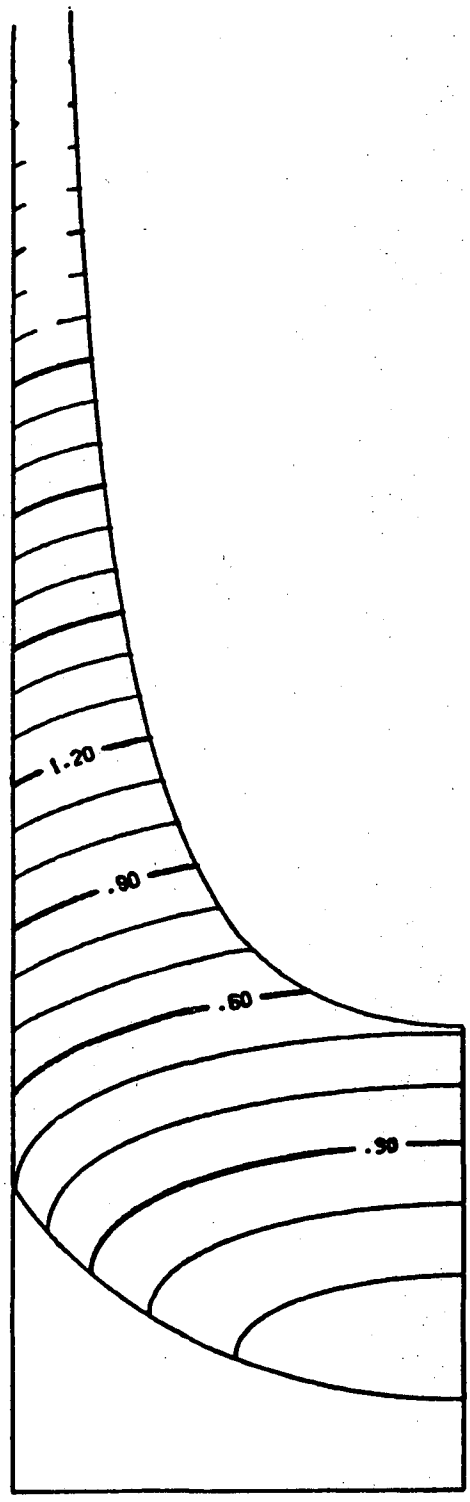

Figure 11. Perspective view for B = 1 from direction (b), $\gamma = 30°$.

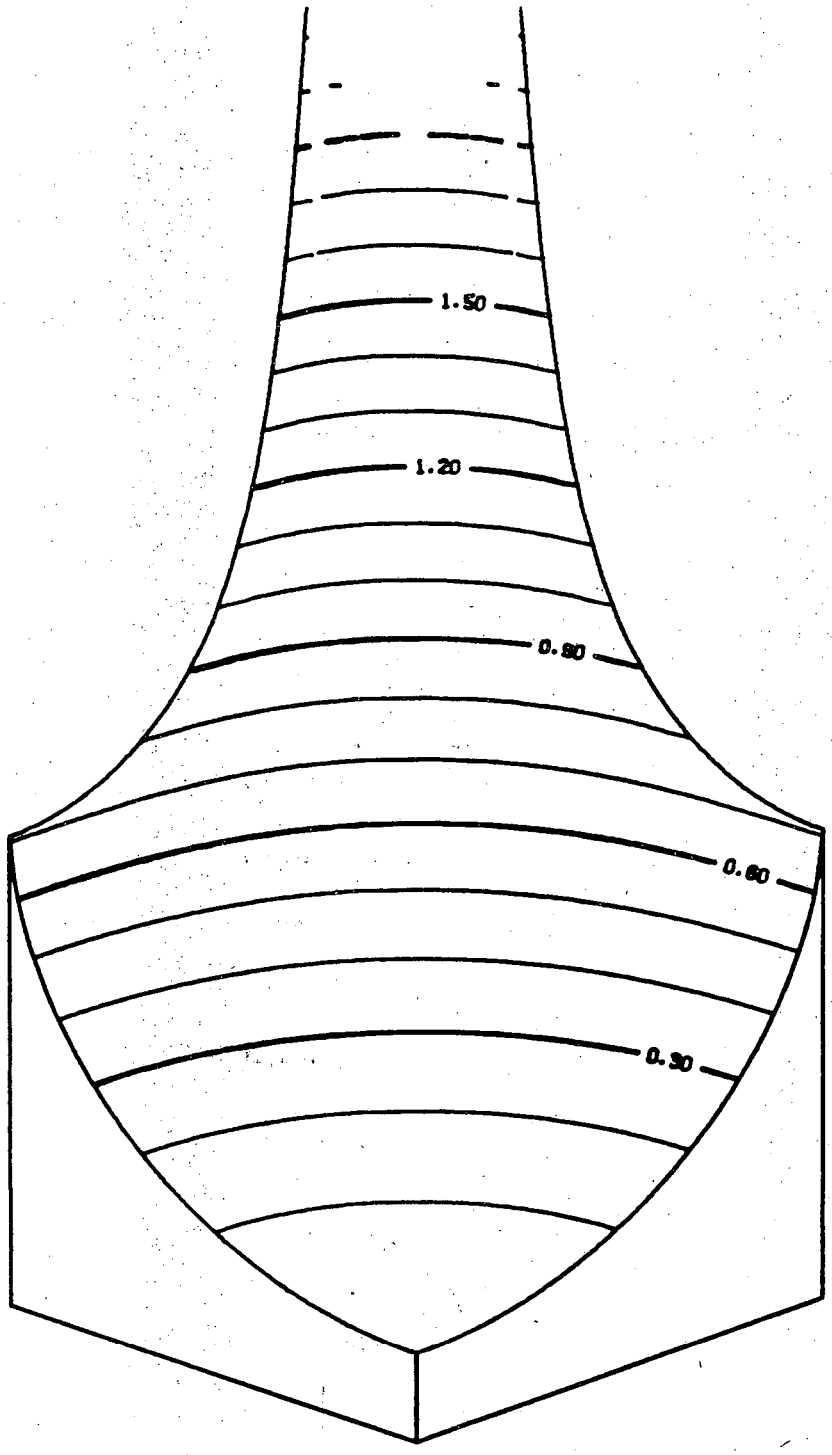

Fig. 12

Perspective view for B = 1 from direction (a), γ =0°.

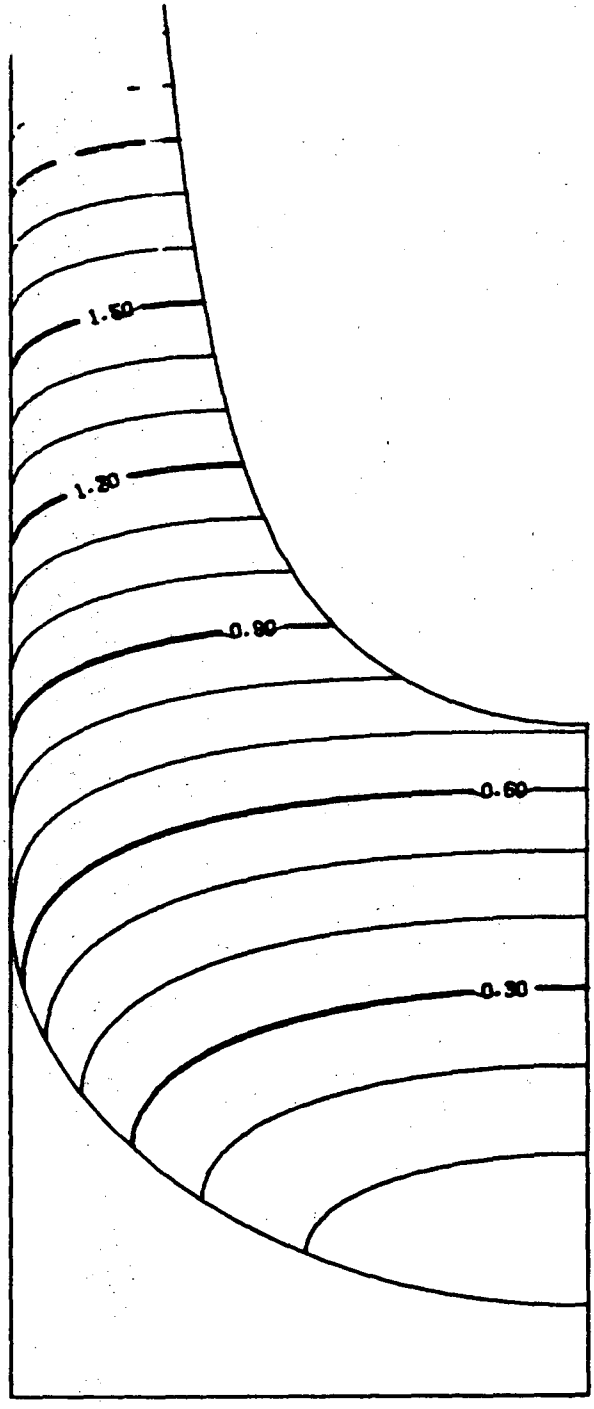

Fig. 13

Perspective view for B = 1 from direction (b), $\gamma = 0°$.

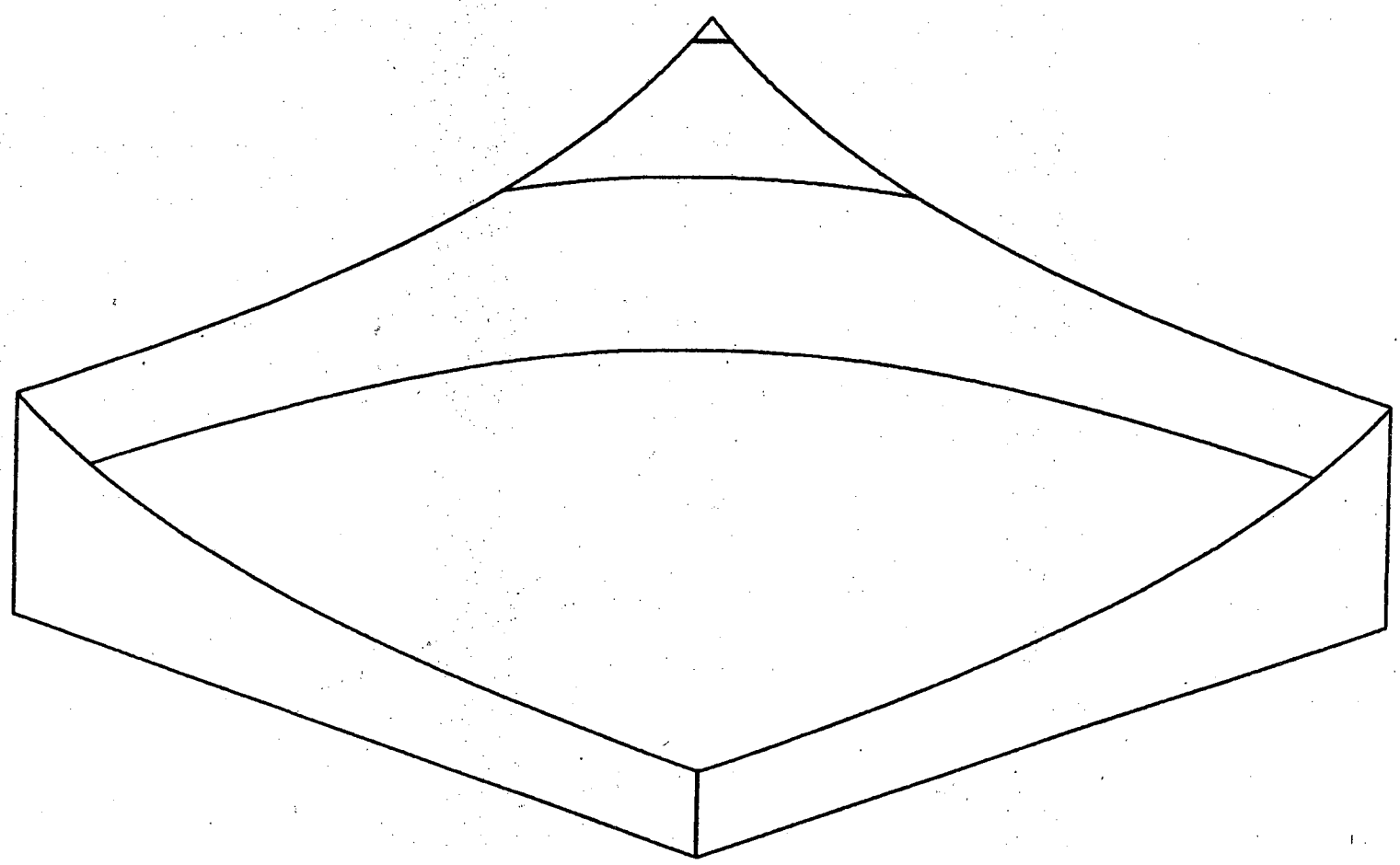

Figure 14

Perspective view for B = 10 from direction (a), $\gamma = 60^{o}$.

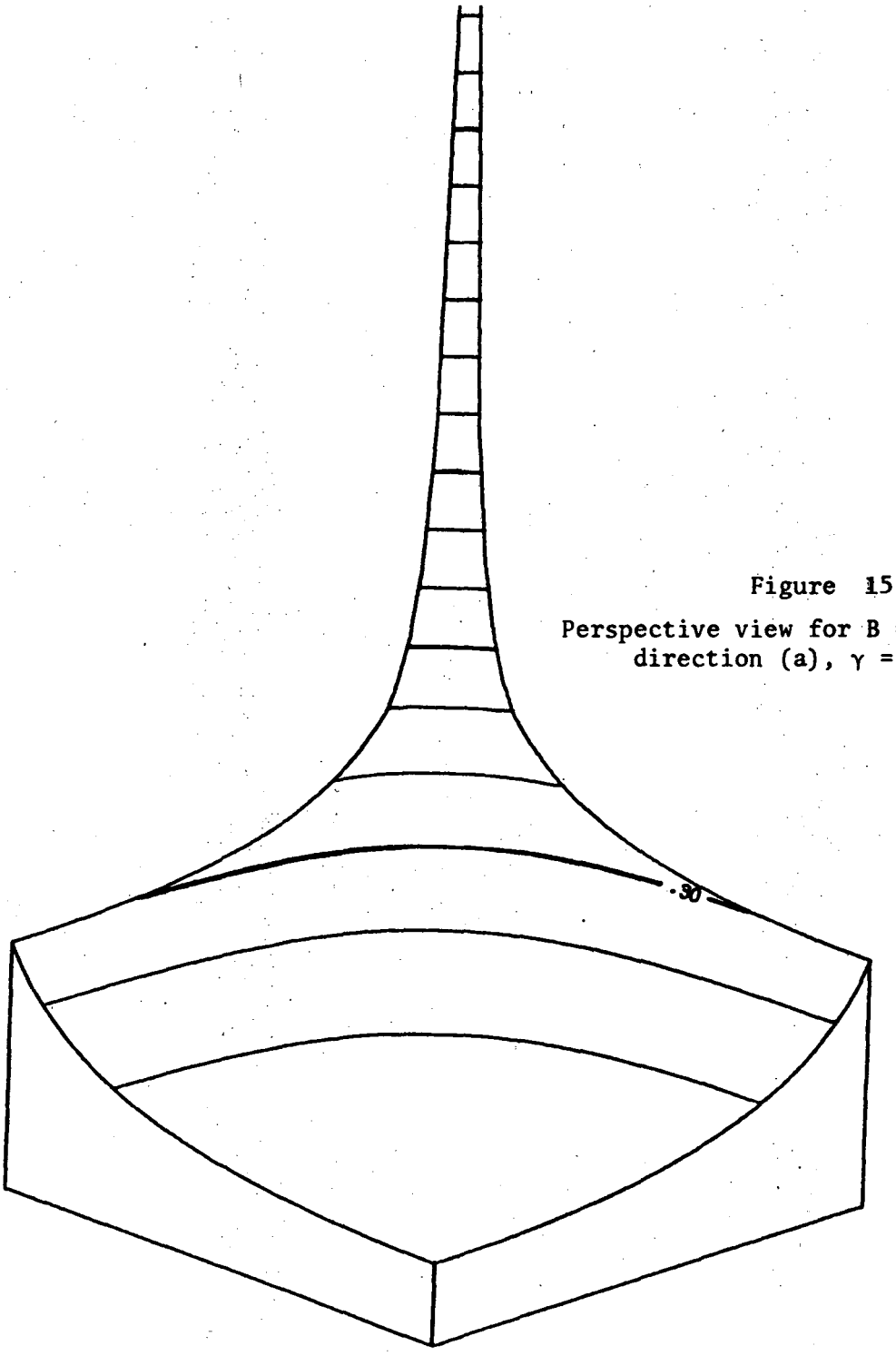

Figure 15

Perspective view for B = 10 from direction (a), $\gamma = 30^{o}$.

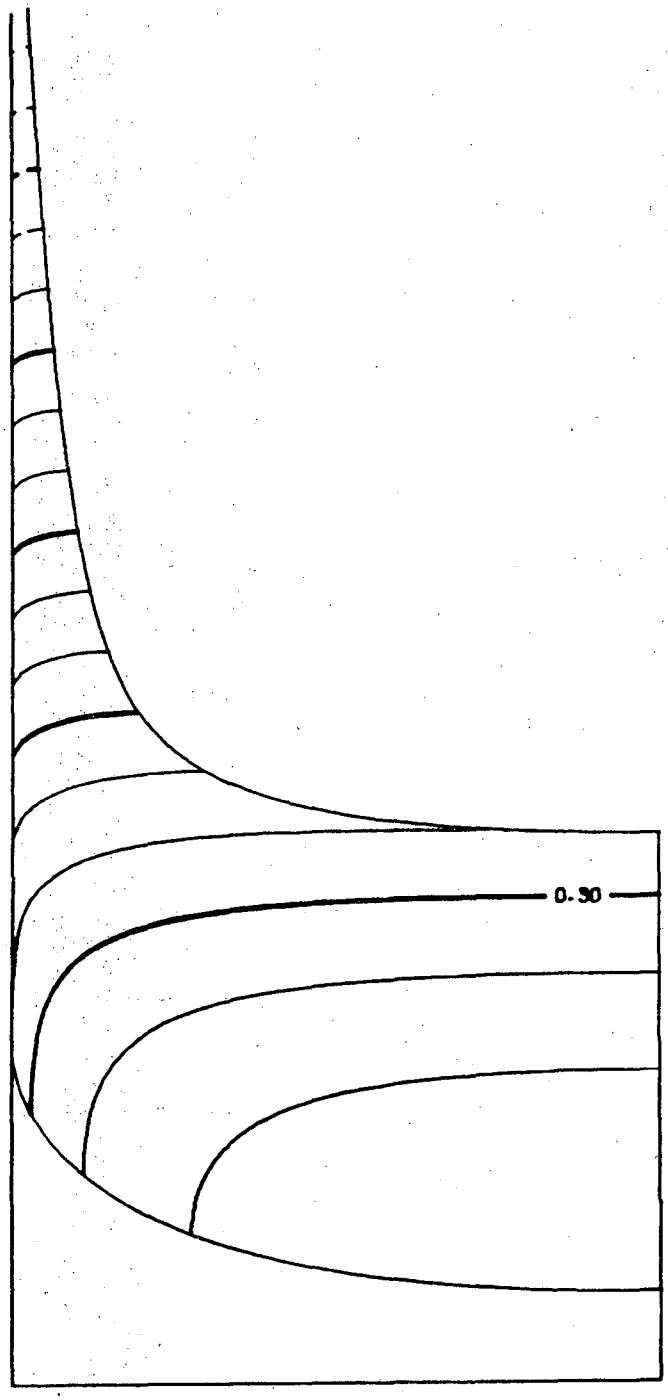

Fig. 16

Perspective view for B = 10 from direction (b), $\gamma = 30°$.

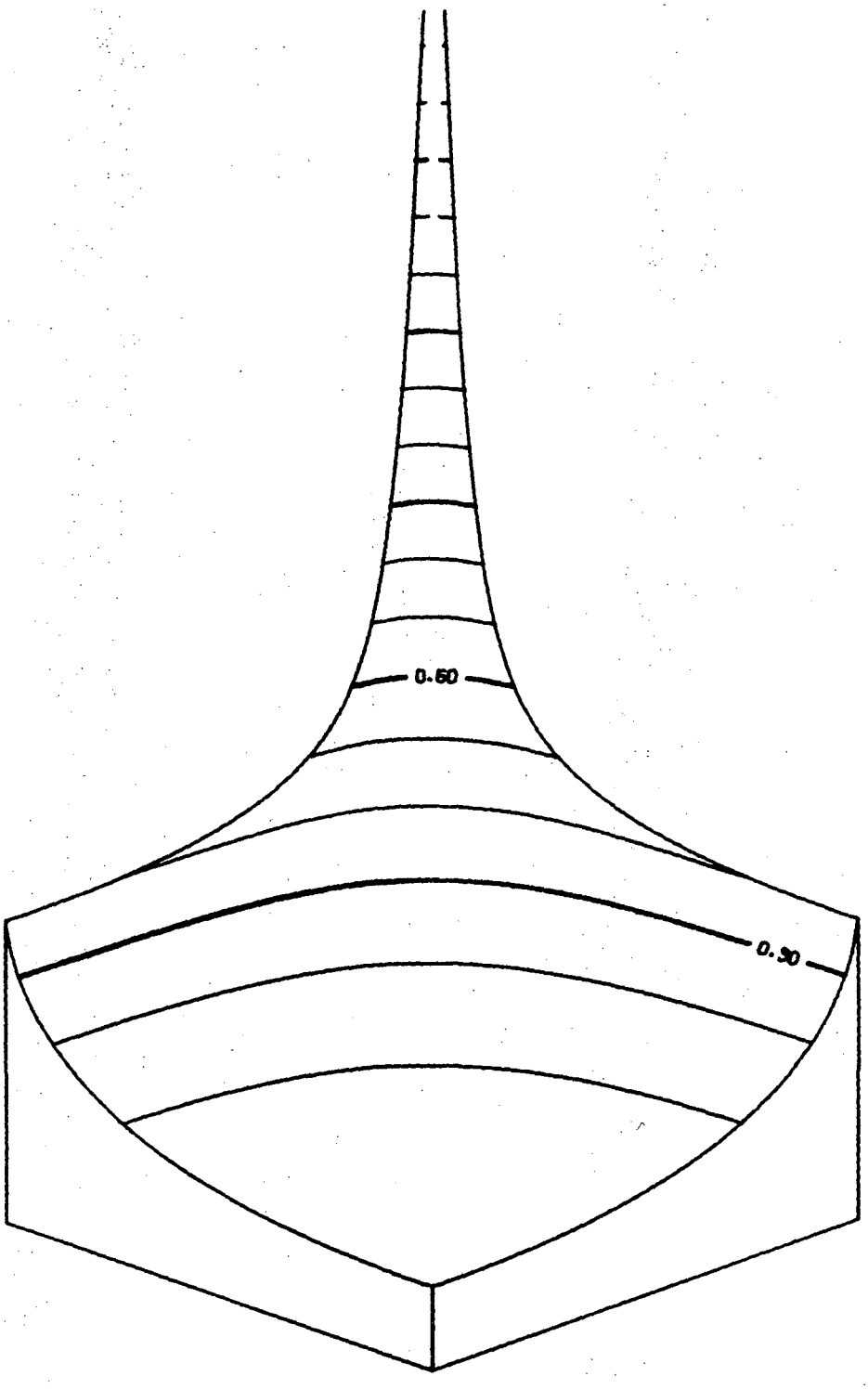

Fig. 17

Perspective view for B = 10 from direction (a), $\gamma = 0°$.

Figure 18

Perspective view for B = 10 from direction (b), $\gamma = 0°$

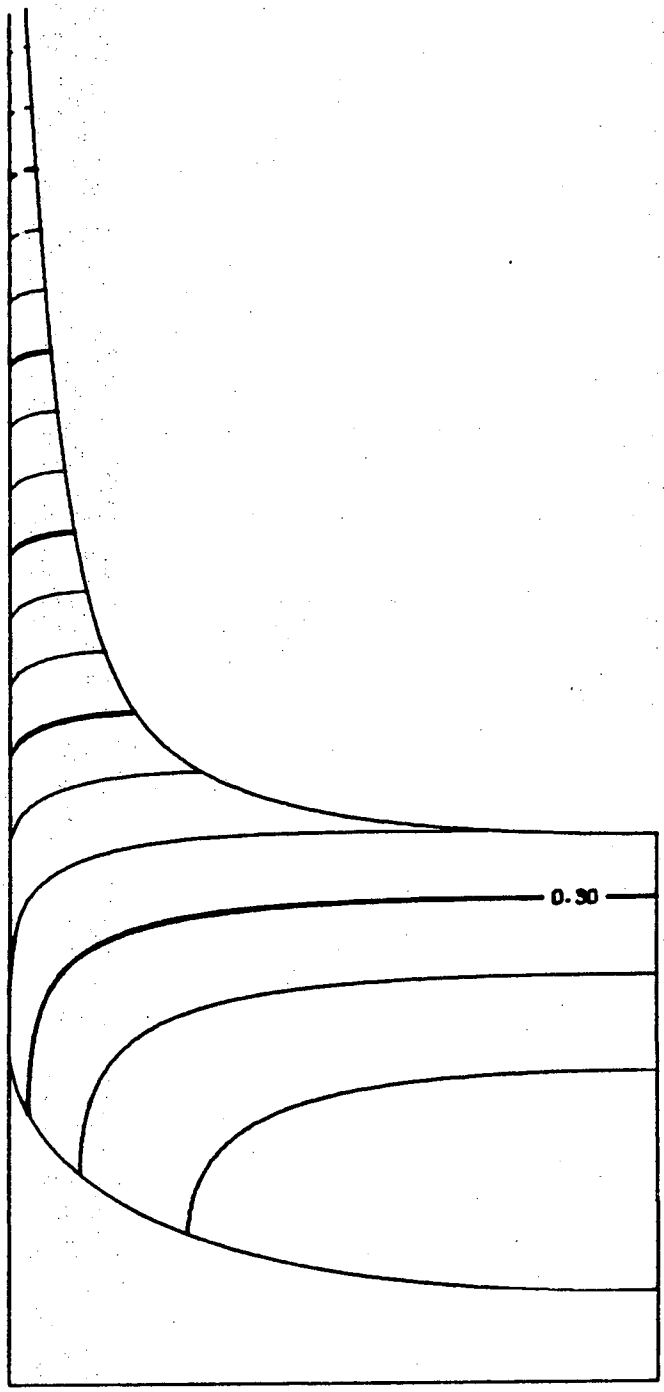

Acknowledgments

This work was supported in part by the National Aeronautics and Space Administration and by the U. S. Department of Energy.

References

[1] N. Albright, "Numerical computation of capillary surfaces on irregularly shaped domains by a finite element method," Report LBL-6136, Lawrence Berkeley Laboratory, University of California (1977).

[2] R . E. Bank, A FORTRAN implementation of the generalized marching algorithm, Trans. Math. Software (to appear).

[3] P. Concus, "Numerical solution of the minimal surface equation," Math. Comp. 21 (1967), 340-350.

[4] P. Concus, "Numerical solution of the minimal surface equation by block non-linear successive overrelaxation," Information Processing 68, Proc. IFIP Congress 1968, North-Holland, Amsterdam (1969), 153-158.

[5] P. Concus and R. Finn, "On a class of capillary surfaces," J. Analyse Math. 23 (1970), 65-70.

[6] P. Concus and R. Finn, "On capillary free-surfaces in the absence of gravity," Acta Math. 132 (1974), 179-198.

[7] P. Concus and R. Finn, "On capillary free surfaces in a gravitational field," Acta Math. 132 (1974), 207-223.

[8] P. Concus, G. H. Golub, and D. P. O'Leary, "Numerical solution of nonlinear elliptic partial differential equations by a generalized conjugate gradient method," Computing (to appear).

[9] R. Finn and C. Gerhardt, "The internal sphere condition and the capillary problem" Ann. Mat. Pura ed Applicata CXII (1977), 13-31.

[10] J. M. Ortega and W. C. Rheinboldt, "Iterative Solution of Nonlinear Equations in Several Variables," Academic Press, New York (1970).

[11] R. Varga, "Matrix Iterative Analysis," Prentice-Hall, New Jersey (1962).

TECHNICAL INFORMATION DEPARTMENT
LAWRENCE BERKELEY LABORATORY
UNIVERSITY OF CALIFORNIA
BERKELEY, CALIFORNIA 94720